JGR Atmospheres

RESEARCH ARTICLE
10.1029/2019JD032155

Present Temperature, Precipitation, and Rain-on-Snow Climate in Svalbard

Siiri Wickström[1,2], Marius O. Jonassen[1,2], John J. Cassano[3], and Timo Vihma[1,4]

[1]Department of Arctic Geophysics, University Centre in Svalbard, Longyearbyen, Norway, [2]Geophysical Institute, University of Bergen, Bergen, Norway, [3]Department of Atmospheric and Oceanic Sciences (ATOC), University of Colorado Boulder, Boulder, CO, USA, [4]Finnish Meteorological Institute, Helsinki, Finland

Key Points:
- Winter and spring temperature and precipitation conditions in Svalbard are most sensitive to the synoptic flow direction
- At the northern and eastern parts of Svalbard the precipitation intensity appears to depend on upstream sea ice conditions
- Rain-on-snow events in Svalbard have the largest spatial coverage under southwesterly synoptic flow

Supporting Information:
- Supporting Information S1

Correspondence to:
S. Wickström,
siiri.wickstrom@unis.no

Citation:
Wickström, S., Jonassen, M. O., Cassano, J. J., & Vihma, T. (2020). Present temperature, precipitation, and rain-on-snow climate in Svalbard. *Journal of Geophysical Research: Atmospheres*, *125*, e2019JD032155. https://doi.org/10.1029/2019JD032155

Received 11 DEC 2019
Accepted 10 MAY 2020
Accepted article online 17 MAY 2020

Abstract The Svalbard Archipelago has undergone rapid warming in the recent decades leading to warmer and wetter winter conditions. This study relates the present (2013–2018) 2 m temperature, precipitation, and rain-on-snow (ROS) climate in Svalbard to different atmospheric circulation (AC) types utilizing the high-resolution numerical weather prediction model Application of Research to Operations at Mesoscale (AROME)-Arctic. We find that the 2 m median temperatures vary most across AC types in winter and spring and in summer they vary the least. In all seasons the 10th percentile 2 m temperatures are above 0°C with southwesterly AC types over Svalbard. In comparison, the relationship between AC type and precipitation varies more spatially, with most accumulated precipitation and highest median precipitation intensities with onshore flow over open water. Our results suggest that sea ice explains a large part of the local variability in both 2 m temperature and precipitation. In the studied period ROS is a frequent phenomenon up to 150 m above sea level (ASL) on land, with most events in the southwestern parts of the archipelago (57 cases during five winter seasons). ROS events in winter occur predominantly with AC types from the southerly sector or during a low-pressure center/trough passage. The southwesterly cyclonic AC type, with a low-pressure center west of Svalbard, is the most frequent AC type for ROS events. In addition to being the most frequent, the southwesterly AC has the largest spatial coverage of ROS.

Plain Language Summary The Svalbard Archipelago has undergone rapid warming in the recent decades leading to warmer and wetter winter conditions. This study relates the present (2013–2018) 2 m temperature, precipitation, and rain-on-snow (ROS) climate to different atmospheric circulation (AC) types utilizing the high-resolution numerical weather prediction model Application of Research to Operations at Mesoscale (AROME)-Arctic. We found that winter and spring 2 m median temperatures vary most across AC types and in summer they vary the least. Our results suggest that sea ice explains a large part of the local variability in both 2 m temperature and precipitation. In the studied period ROS is a frequent phenomenon up to 150 m ASL on land, with most events in the southwestern parts of the archipelago (57 cases during five winter seasons). The majority of these events occur in southwesterly cyclonic AC type, with a low-pressure center west of Svalbard. In addition to being the most frequent, the southwesterly AC has the largest spatial coverage of ROS.

1. Introduction

The Svalbard Archipelago and its rapidly changing climate have received a lot of attention, both scientifically and among the media in recent years. The mean winter 2 m air temperature at Svalbard Airport (close to Longyearbyen, the largest settlement in Svalbard) has increased by 7.8°C in the period 1971–2017 (Table 4.1.3 in Hanssen-Bauer et al., 2019). The annual increase averaged over all Svalbard is 4.0°C for the same time period (0.87°C per decade) (Hanssen-Bauer et al., 2019). In comparison, the observed global temperature rise is only 0.18°C per decade, translating to 0.83°C warming in the same period, making Svalbard a hot spot of climate change to date. Several studies have addressed the rapid warming rates and the Svalbard temperature climatology (Førland et al., 2012; Gjelten et al., 2016; Isaksen et al., 2016; Nordli et al., 2014). Alongside these temperature changes, the frequency of extreme precipitation events has been documented to increase (Łupikasza et al., 2019; Peeters et al., 2019; Rinke et al., 2017; Serreze et al., 2015; Vikhamar-Schuler et al., 2016). In particular, warm winter events resulting in rain-on-snow (ROS) have drawn attention due to their potential consequences for the cryosphere, ecosystems, and infrastructure in

Svalbard (Hansen et al., 2019; Peeters et al., 2019; Serreze et al., 2015), elsewhere in the Arctic (Bieniek et al., 2018; Forbes et al., 2016), and at lower latitudes (McCabe et al., 2007).

The above-mentioned ROS events are typically short-lived events that occur with extratropical cyclone passages during the winter season (Graham et al., 2017; Rinke et al., 2017). Hence, changes in both the large-scale atmospheric circulation (AC) and the properties of the air masses advected by these synoptic systems are key to understanding ROS events in Svalbard. Rinke et al. (2017) documented an increase in winter season "weather bombs," strong extratropical cyclones, entering the Fram Strait with warm and moist air masses. Studies have also shown that the winter season cyclone density around Svalbard has had a positive trend over the last decades (Rudeva & Simmonds, 2015; Wickström et al., 2019; Zahn et al., 2018). The increase is hypothesized to be a result of the cyclones penetrating farther north in a warmer climate (Tamarin-Brodsky & Kaspi, 2017), which is likely related to sea ice retreat and the resulting local increase in baroclinicity (Koyama et al., 2017).

The rapid warming rates are a consequence of the ongoing "arctic amplification," which refers to the Arctic warming up at about twice the rate of the global mean (Serreze et al., 2008; Serreze & Barry, 2011). The arctic amplification is a sum of several contributing factors: the background warming due to increased atmospheric CO_2 concentrations, changes in the large-scale AC (Overland & Wang, 2016), changes in sea ice extent (Dai et al., 2019), and increased water vapor content in the troposphere (Park et al., 2015) together with changes in both atmospheric boundary layer stability and cloud cover (Graversen et al., 2014; Pithan & Mauritsen, 2014).

Svalbard is located at the main gateway of both atmospheric and oceanic heat transport into the Central Arctic. In the extratropics, cyclone activity is the main atmospheric mechanism of poleward heat transport, transporting warm and moist air masses, together with high winds and precipitation (Trenberth & Stepaniak, 2003). As the North Atlantic storm track is stronger than its Pacific counterpart (Schlichtholz, 2018), the majority of the atmospheric heat flows poleward via the high-latitude North Atlantic, either into the Barents Sea or through the Fram Strait (Zhang et al., 2004). Like in the atmosphere, the Atlantic sector facilitates for most poleward heat transport in the ocean in the northern hemisphere both through the Fram Strait and via the Barents Sea (Aagaard & Greisman, 1975; Carmack et al., 2015).

Furthermore, local changes in upwind conditions affect the air masses reaching Svalbard. The regions around Svalbard have lost a considerable portion of their winter sea ice extent in recent decades. This is especially true for the regions north (Onarheim et al., 2014) and east of the archipelago—in the Barents Sea (Smedsrud et al., 2013). Regions losing sea ice are converted from sink to source regions of atmospheric heat and moisture—having a large impact on local and regional climate (Smedsrud et al., 2010). Isaksen et al. (2016) showed that six AC types, mainly from the northern and eastern sectors, contributed to the warm surface air temperature anomaly in 2001–2015, when compared to the 1971–2000 period, matching well with the upwind sea ice reduction in the east and north of Svalbard.

The quality of numerical weather prediction products for Arctic regions has increased substantially over the last few years (e.g., Bauer & Jung, 2016; Bromwich et al., 2016). However, challenges still remain related to for example poor understanding and modeling of processes of stable boundary layers (Køltzow et al., 2019; Zilitinkevich & Esau, 2005) and atmosphere-sea ice coupling (Vihma et al., 2014), and to the sparse network of observations causing uncertainties in the model initialization (Vihma et al., 2014).

In response to these challenges and shortcomings, and an increased demand for accurate weather forecasts in the Arctic, the AROME-Arctic weather model (AROME = Application of Research to Operations at Mesoscale) has been implemented and is now run operationally by the Norwegian Meteorological Institute for a single domain centered on Svalbard. Several validation studies have shown AROME-Arctic to perform well in the high latitudes (Køltzow et al., 2019; Müller, M., Batrak, Y., et al., 2017; Müller, M., Homleid, M., et al., 2017). Data from this high-resolution (2.5 km horizontal grid spacing) operational model enable detailed studies of the complex air-sea-ice interactions in this region. The model also allows us to study regions outside the observational network. This is especially valuable in the central and eastern parts of Svalbard, as the majority of the observation network is concentrated along the west coast.

By combining the AROME-Arctic and an AC data set (Niedźwiedź, 2013) for the time period January 2013 to December 2018, we present seasonal climatologies of different AC types (synoptic situations) and the

relation between these synoptic situations and 2 m air temperature and precipitation. One of our main objectives is to present the statistics on the synoptic situations giving rise to winter ROS conditions (situations with daily accumulated precipitation of 1 mm or more and temperatures at or above 0°C during winter (December–February, DJF)). The time period studied is relatively short but allows us to address the regional climate in its present state.

We have structured the paper as follows: the next section, section 2, presents the data sets and methods. Thereafter, the first part section 3 is devoted to the seasonal climatology of the AC types and the temperature and precipitation distributions between these AC types. The second part of section 3 presents statistics on ROS events in relation to the AC types, focusing on five different geographical locations in Svalbard. Section 4 discusses the results, and section 5 concludes the study.

2. Data and Methods

2.1. AC Types

The backbone of this study is the daily AC type classification for Svalbard (the"Niedźwiedź Classification"; Niedźwiedź, 2013). This classification was generated manually based on German synoptic maps published in the Deutscher Wetterdienst Archives (http://www.wetter3.de/Archiv/archiv_dwd.html). The synoptic situations are classified into 21 different AC types divided into the main geostrophic wind direction assessed from the mean sea level pressure (MSLP) field. The "Niedźwiedź Classification" uses the same methodology as the well-known AC classification made for the British Isles (Lamb, 1972).

In the original data set, the AC types are denoted with a capital letter indicating the geostrophic wind direction (e.g., N = northern, NE = northeastern) and a lowercase letter indicating if the synoptic situation is driven by a cyclone (c) or an anticyclone (a). In addition to eight cyclonic (Nc, NEc, Ec, SEc, Sc, SWc, Wc, and NWc) and eight anticyclonic AC types, the data set includes four nondirectional types (Ca = high-pressure center over or very near Svalbard, Ka = high-pressure ridge, Cc = low-pressure center over or very near Svalbard, and Bc = cyclonic trough) and one unclassified AC type, X. In the results section we also defined our own cyclonic nondirectional AC type Zc, a combination of Bc and Cc (Bc + Cc). In this work we have chosen to mark the cyclonic AC types only with a capital letter for the directional AC types and keep the lowercase "a" for the anticyclonic AC types (e.g., SW = southwesterly geostrophic wind over Svalbard driven by low pressure in the vicinity of Svalbard, SWa = as SW but the flow is driven by high pressure in the vicinity of Svalbard).

2.2. AROME-Arctic

To study the variability in regional temperature and precipitation conditions with different AC types (described above), we have used the operational weather model AROME-Arctic from the Norwegian Meteorological Institute. AROME-Arctic is a regional mesoscale forecasting system covering the European Arctic, including the northern part of Norway, the Barents Sea, surrounding islands, and parts of the Greenland Sea. AROME-Arctic has a horizontal grid spacing of 2.5 km and 65 levels in the vertical reaching up to 9 hPa (24 km). Of these levels, 20 model levels are located below 1 km above the ground (the lowermost at approximately 11 m), enabling the model to resolve fine-scale boundary layer structures. The model is run operationally four times a day at 0000, 0600, 1200, and 1800 UTC with a forecast range of 66 hr and an output frequency of 1 hr. A detailed description of the model's physics and setup can be found in Bengtsson et al. (2017), Müller, M., Batrak, Y., et al. (2017), and Müller, M., Homleid, M., et al. (2017). For this study, operational forecasts starting at 0000 UTC with forecast lengths up to 24 hr were used.

To combine the AC type classification with the AROME-Arctic data, we calculated daily means of mean sea level pressure, 2 m air temperature and precipitation intensity from the model output.

2.3. Automatic Weather Stations and Sea Ice Observations

To study the spatial distribution and variability in precipitation, temperature, and wind with the different AC types, we extracted model data from five different locations. These are the locations of the following, World Meteorological Organization (WMO) standard automatic weather stations (AWS) in Svalbard: the Verlegenhuken (N) station in the north, the Edgeøya (E) station in the east, the Sørkappøya (S) station in the south, the Svalbard Airport station (C), considered as the central station, and the Ny-Ålesund (W)

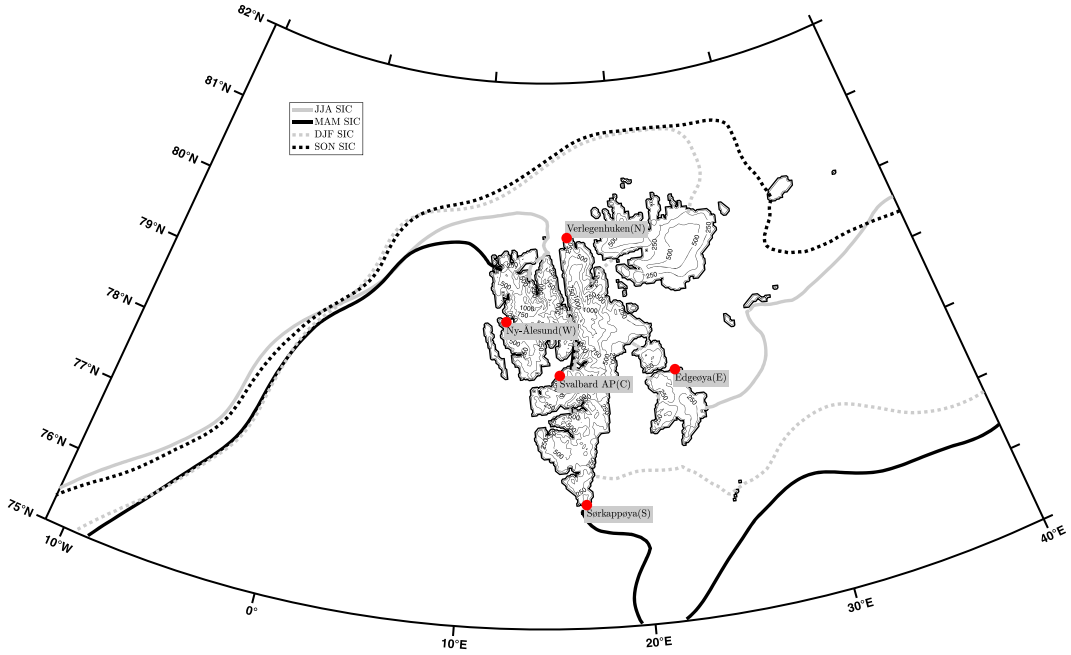

Figure 1. The Svalbard archipelago with the five AWS sites and the mean seasonal sea ice edge (15% concentration) for summer (JJA), spring (MAM), winter (DJF), and autumn (SON) for the years 2013–2018. Svalbard AP refers to the Svalbard Airport station.

station in the west (Figure 1). We note that even though we have chosen to call the Svalbard Airport "Central," it is on the west side of the highest mountain peaks and ice caps in the central parts of Spitsbergen. Hence, it is arguably most representative of west coast conditions in the fjord system (Figure 1).

To match the model data, daily means of the AWS data are used for model validation.

Of the five stations presented above, the Svalbard Airport and Ny-Ålesund stations have manual precipitation measurements along with the AWSs. In this work the manual precipitation measurements are utilized, as these data sets have fewer gaps in comparison to the automated precipitation measurements.

The sea ice extent data used are from the Operational Sea Surface Temperature and Sea Ice Analysis (OSTIA) 2012, based on passive microwave satellite observations. The sea ice extent (defined as 15% concentration) is at its minimum in autumn (September–November, SON) with the mean 2013–2018 ice edge running north of Svalbard, close to 81°N (Figure 1). The mean sea ice extent around Svalbard is largest in spring (March–May, MAM) with only the west coast being ice free. The winter (DJF) ice extent is similar to that of MAM, with the exception of an ice-free tongue north of Svalbard aligning with the autumn ice edge. In summer (June–August, JJA) the mean ice edge retreats to 77.5°N in the Barents Sea but still covers most of the northern coast However, especially in JJA, the interannual variability (not shown) is large over the six consecutive years studied in this work.

2.4. ROS Events

We define ROS events as DJF days that have a mean daily temperature at or above 0°C and a daily accumulated precipitation of 1 mm or more. We chose this definition to capture possible events when above-freezing temperatures and precipitation (rain) co-occur in DJF. These events cause melting and have potentially large consequences for both the arctic cryosphere and biosphere, in addition to being a societal challenge with regard to people and infrastructure.

We chose not to include MAM in the ROS analysis, because the majority of the ROS events were found in May in this season (not shown). Furthermore, May is at the transition of winter and summer conditions and hence ROS events can typically contribute to melt onset. This does not have the same high-impact potential as the ROS events occurring during winter when the snowpack refreezes after the rain. March

Table 1
Validation Statistics of AROME-Arctic for Rain-on-Snow Events in DJF 2013–2018 Using the Five Observation Stations (the Columns) Shown in Figure 1 as Reference

	Verlegenhuken (N)	Edgeøya (E)	Sørkappøya (S)	Svalbard airport (C)	Ny-Ålesund (W)
Num. ROS events in model	6	6	47	28	21
Hit rate T 2 m	100%	83%	83%	86%	91%
RMSE T2m	2.0°C	4.7°C	0.3°C	0.6°C	0.6°C
Mean bias T2m	−0.1°C	−0.2°C	0.4°C	−0.8°C	−0.7°C
Hit rate 1 mm RR (missed events)	—	—	—	54% (13)	86% (3)
RMSE RR	—	—	—	4.9 mm	10.6 mm
Mean bias RR	—	—	—	−2 mm	−6.3 mm

Note. RR is precipitation intensity (mm per 24 hr).

and April are the driest months in Svalbard, and we only found a handful ROS events in these months. Hence, we argue that the DJF is the season with the highest impact ROS events and we therefore chose to only focus on this season for the ROS events.

We are aware that some of these "warm and wet" winter events are not necessarily actual ROS events, as we do not have the means to (a) assure that the surface is covered by snow or (b) that the precipitation is falling as rain. Further, since we are working with daily mean values, we cannot guarantee that the above-freezing temperatures and precipitation occur simultaneously. However, given the typical structure of extratropical cyclones, we do believe that our definition will capture extremely mild winter precipitation events produced by AROME-Arctic, and we will refer to these events as ROS events in the following discussion.

2.5. Model Validation

We have done basic validation of the AROME-Arctic for ROS events at all five stations and precipitation for these events at selected stations on Spitsbergen, the main island of the archipelago, where data are available (Ny-Ålesund and Longyearbyen). As documented by Køltzow et al. (2019), AROME-Arctic generally performs well with regard to 2 m air temperatures. We find that for all stations, over 80% of the ROS events identified based on the model results had daily observed mean temperatures at or over 0°C, 100% of the time for Verlegenhugen (6 cases) in the north and 91% for Svalbard Airport (28 cases) and 86% for Ny-Ålesund (21 cases) in the center and west. For the Sørkappøya (47 cases) and Edgøya (6 cases) stations in the south and in the east, the corresponding number is 83% (Table 1).

When the model captures an observed event of above-freezing winter temperatures, it underestimates the daily mean temperature at the south, west, and central stations on average by −0.3°C, −0.8°C, and −0.7°C, respectively. With the relatively few cases at the north (six cases) and east (six cases) stations the bias (mean error) is very close to 0.

Table 1 shows that with a threshold of 1 mm precipitation for ROS events, the hit rate is 54% and 86% at the central and western station, respectively. When lowering the threshold of the observed precipitation to 0.2 mm, the corresponding hit rates are 71% (Svalbard Airport) and 90% (Ny-Ålesund). The root-mean-square errors (RMSEs) are 4.9 and 10.6 mm per ROS event for these stations, respectively, with biases of −2 and −6.3 mm (model underestimating the precipitation).

3. Results

3.1. Seasonal Climatologies

3.1.1. AC Distribution

As a consequence of Svalbard's location at the periphery of the North Atlantic storm track, the vast majority of the AC types are cyclonic in all seasons (Figure 2). An exception to this is the northeasterly flow in MAM, which is predominantly driven by the anticyclonic AC type. Also, the frequency of a pressure ridge (Ka) over Svalbard exceeds that of a pressure trough (Bc) in all seasons but DJF. In general, flow from the easterly sectors (NE, E, and SE) prevails over Svalbard and flow from the west and northwest is the least frequent in all seasons except in JJA. The easterly dominance is strongest in DJF, with a combined frequency of about 45%, close to equally divided between a flow from northeast (NE), east (E), and southeast (SE) (~15% each, Figure 2a). The occurrence of the anticyclonic AC type is less than 5% for all of these flow directions, and hence, the majority of

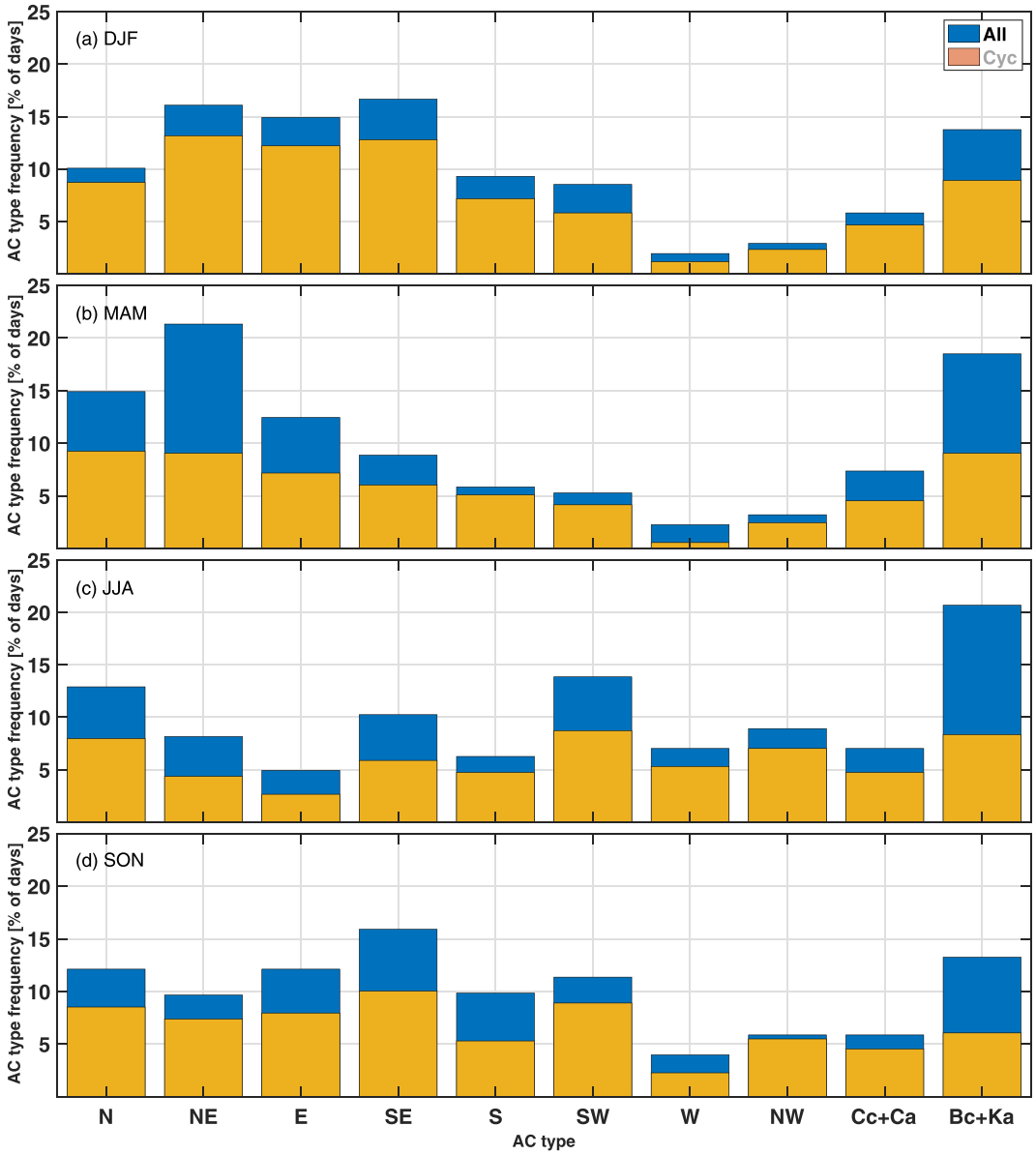

Figure 2. (a–d) Seasonal atmospheric circulation (AC) type frequencies (% of days per season) for the years 2013–2018.

the winter season flow is driven by a cyclone in the Barents Sea or south of Svalbard (Figure S1 in the supporting information). The AC types accounting for pressure ridges and troughs (Ka and Bc, respectively) have the second largest contribution after flow from the easterly sector (NE, E, and SE) in DJF. In line with an active storm track during DJF, the pressure trough occurrence exceeds that of a ridge. Flow from the west and northwest are the least common in DJF with an occurrence frequency less than 2.5% of the time.

In MAM the most frequent AC type is northeast and in SON southeast (Figures 2b and 2d). More than half of the northeast circulation in MAM is of the anticyclonic AC type NEa, resulting from a strong Greenland high, reaching all the way over the Fram Strait (Figure S2). In general, compared to DJF, the AC type is dominated more by northerly flow in MAM and southerly flow in SON. Compared to DJF and MAM, the AC types are more evenly distributed in SON.

In JJA the North Atlantic storm track is at its weakest, and over 20% of the time the AC is characterized by a pressure ridge or trough above Svalbard. Unlike in the other seasons, southwesterly flow is the most frequent AC type in JJA, after Bc and Ka. In general, this season has the most even distribution of the AC types.

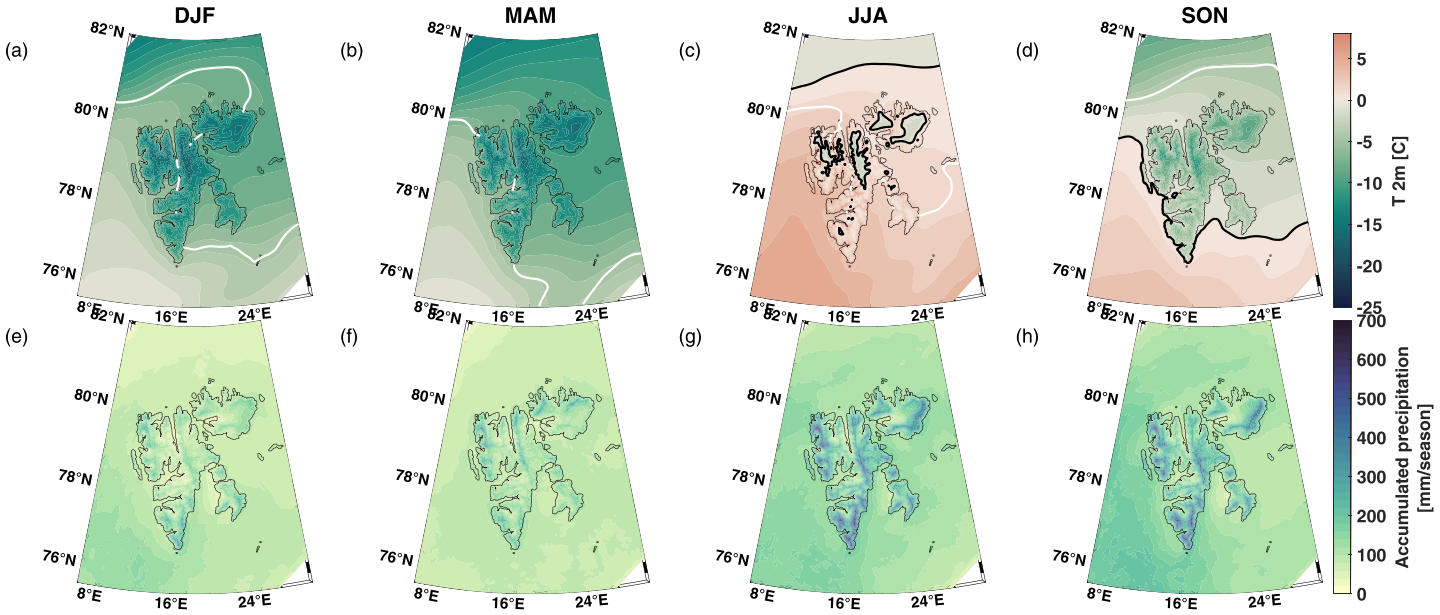

Figure 3. Maps of (a–d) seasonal mean 2 m temperatures (°C) and (e–h) accumulated precipitation (mm) for the period 2013–2018. The mean seasonal sea ice edge (15% concentration) is indicated with a white, solid line, and the 0°C isotherm is indicated with a black, solid line (JJA and SON, only).

3.1.2. Temperature and Precipitation

Moving onto the mean seasonal near-surface temperature and precipitation conditions over the study period; as expected, DJF and MAM have the coldest mean seasonal 2 m air temperatures with down to −20°C in the northeastern parts of the archipelago (Figures 3a and 3b). In the west the winters are milder with seasonal means between −5°C and −10°C at the coast, and between 0°C and −5°C over the fjords and the shelf off the west coast. MAM temperatures north of Svalbard are colder compared to DJF. In SON the 0°C isotherm crosses the domain, indicating subzero temperatures on land and north and east of the archipelago, and higher temperatures (0°C to 5°C) in the south and west. The JJA temperatures are above freezing everywhere except at higher elevations in the northern and northeastern parts of the archipelago and north of about 81°N.

The mean seasonal accumulated precipitation is highest in DJF and SON with up to 600 mm per season in the coastal areas, especially in the southwest (Figures 3e and 3h). The ice-free tongue north of Svalbard in DJF is visible as a gradient in the mean seasonal precipitation field, with close to 300 mm per season northwest of Svalbard and values below 100 mm per season beyond the mean seasonal sea ice edge. MAM is the driest of the seasons, with below 50 mm per season in large parts of the central Spitsbergen and over the ocean north and east of the archipelago, which is in line with the mean seasonal sea ice cover being at its maximum at this time of the year. In JJA the precipitation amounts are relatively low, generally below 200 mm per season in the whole domain with slightly higher values on the west coast of Svalbard (up to 250 mm per season) associated with a weakened North Atlantic storm track at this time of year.

3.2. Temperature and Precipitation Variability With AC Type

3.2.1. Temperature

In this section we investigate temperature and precipitation conditions for different AC types at the five different stations. The 2 m temperature variability is generally largest for DJF and MAM at all the stations (Figure 4, Column 1 and 2). The eastern and northern stations have in general very similar 2 m air temperature variability across the different AC types, with the lowest median DJF and MAM 2 m temperatures for all AC types. The southern station has comparatively little variability and has the warmest median for all AC types at about −3°C in DJF and MAM.

With a few exceptions, AC types from the northerly and easterly sectors are associated with colder than average (the "all" box in Figure 4) median temperatures. The warmest 10th percentile temperatures in DJF and MAM are mostly found with the AC types S and SW. The SW AC type has above-freezing 10th percentile

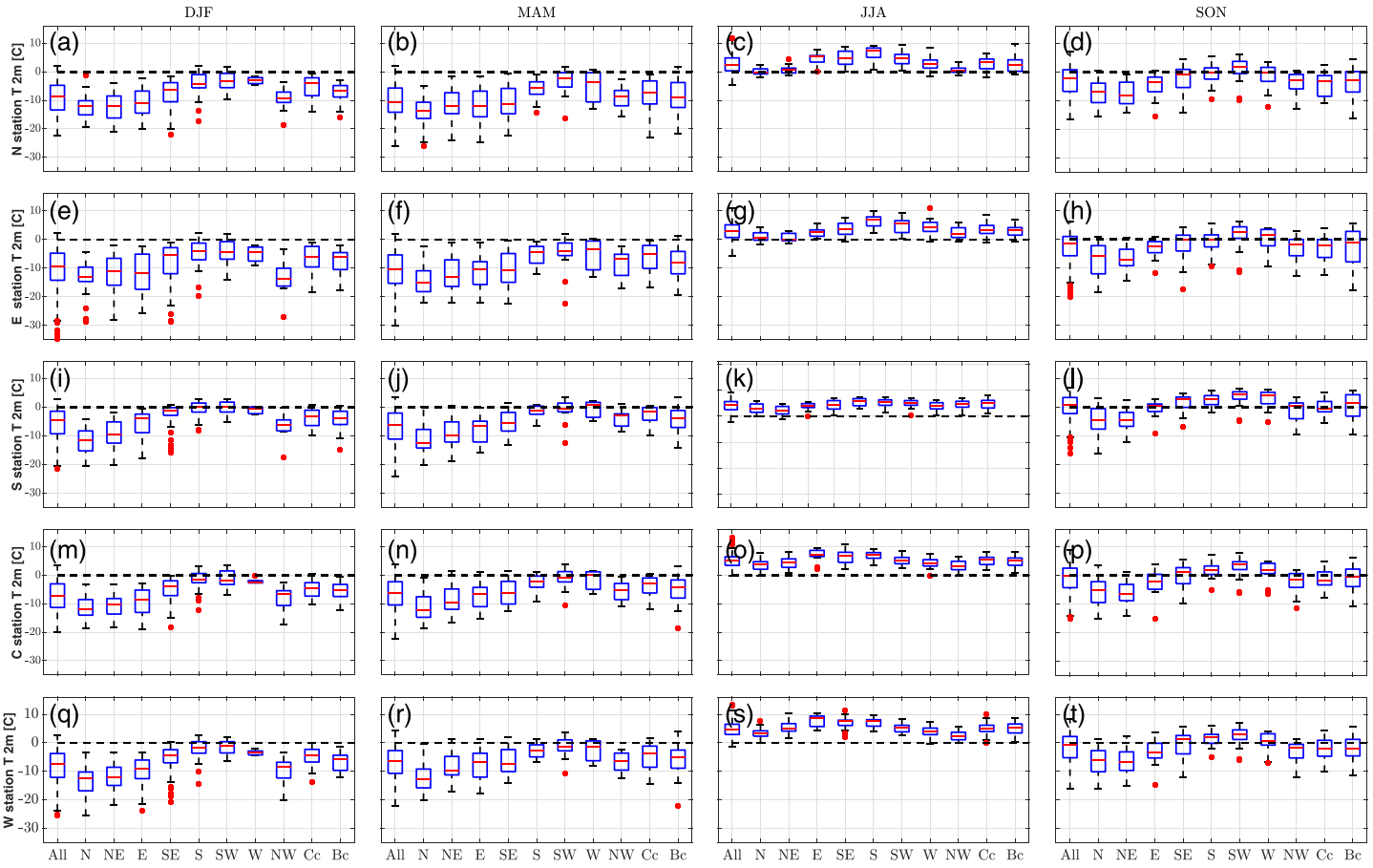

Figure 4. (a–t) Seasonal box and whisker plots of 2 m air temperature (T 2 m) for the cyclonic atmospheric circulation (AC) types during 2013–2018 for all five stations (Figure 1). The solid, red line marks the median, the upper and lower edges of the blue box the 75th and 25th percentiles, the whiskers the 90th and 10th percentiles, and the red crosses are outliers.

temperatures at all stations in all seasons. The S AC type has a below freezing 10th percentile only at the northern and eastern stations in MAM.

JJA features the overall lowest 2 m temperature variability between and within AC types. Also, the spatial variability between the five stations is smallest in JJA. The 2 m air temperature median for all AC types is above 0°C at all stations in JJA, with 3°C in the north and east and around 5°C at the remaining stations.

Focusing on SON, the median 2 m air temperatures are below freezing for all AC types at all five stations, except the southern station Sørkappøya where the SON median is about 3°C (Figure 4l). The variability in SON temperature medians across the different flow types and stations resembles that of DJF, but the temperatures are in general warmer and the variability smaller in SON. The SW AC type median temperatures are the warmest, with above-freezing values at all stations. The southern station has daily 2 m temperature medians above freezing for all AC types, except N, NE, and Cc.

3.2.2. Precipitation

Considering variability in accumulated seasonal precipitation across stations, AC types and seasons the Zc AC type (combined contribution of cyclone centers and pressure troughs) has (with a few exceptions) the largest contribution to the seasonal precipitation at all stations in all seasons (Figure 5). Compared to the other seasons, Zc is the least frequent in SON with 17% of the days (Figure 5f), making it only slightly more common than the SE AC type (15% in SON). In DJF, MAM, and JJA, Zc occurs 19%, 26%, and 28% of the time, respectively.

Moving on to the directional AC types and precipitation intensities, at the northern station most of the precipitation falls with flow from the northerly sectors (N, NE, and NW; Figure 5a). In JJA the SW AC type contributes to over 10% of the seasonal precipitation in the north. At the east station most of the winter

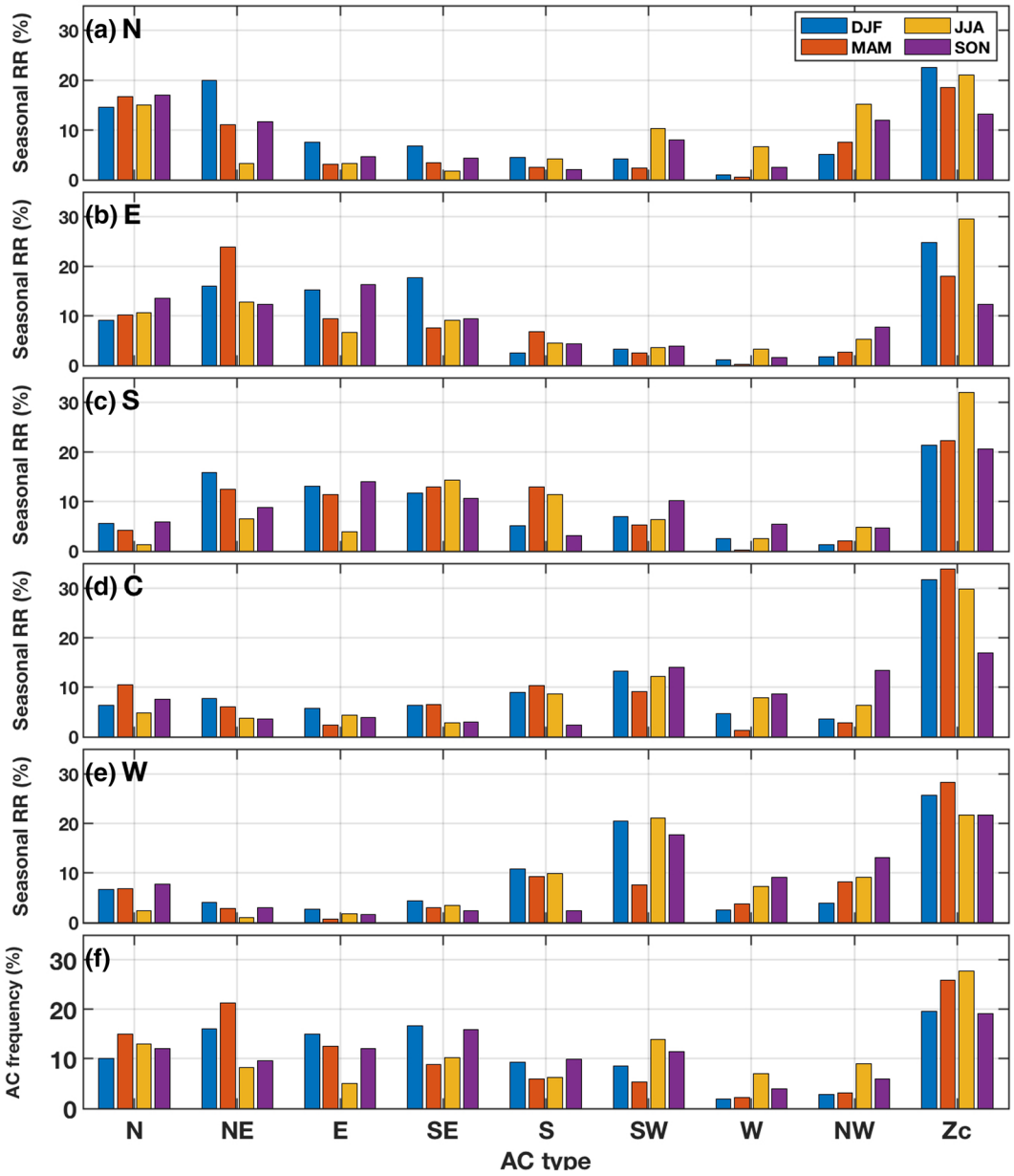

Figure 5. Bar plot of mean seasonal precipitation intensity (RR) with the given AC type at the five stations (a–e) and (f) the seasonal AC distribution in the period 2013–2018 for all five stations.

precipitation falls with the AC types that are the most common in winter (NE, E, and SE), with more than 10% on each of these. At the west and central stations most precipitation falls with the AC type SW.

Figure 6 shows the variability in mean daily precipitation intensities (mm per 24 hr) associated with the cyclonic AC types at the different stations. The general pattern at all stations is that the onshore AC types generally have a higher percentage of precipitation days for a given flow type, pointing to the importance of orography on local precipitation. As an example, at the northern station the N and NW AC types have a very high fraction (%) of precipitation days in DJF, MAM, and SON. For this station, the NW AC type has 92% precipitation frequency in DJF with the 10th percentile at 8 mm per 24 hr. In contrast, the S AC type has a low percentage of precipitation days (49%) with a median of ~1 mm in all seasons.

The precipitation falling with the E AC type has a smaller variability and lower medians in MAM than SON at all stations except the south station. This is likely a reflection of MAM being the driest of the seasons with

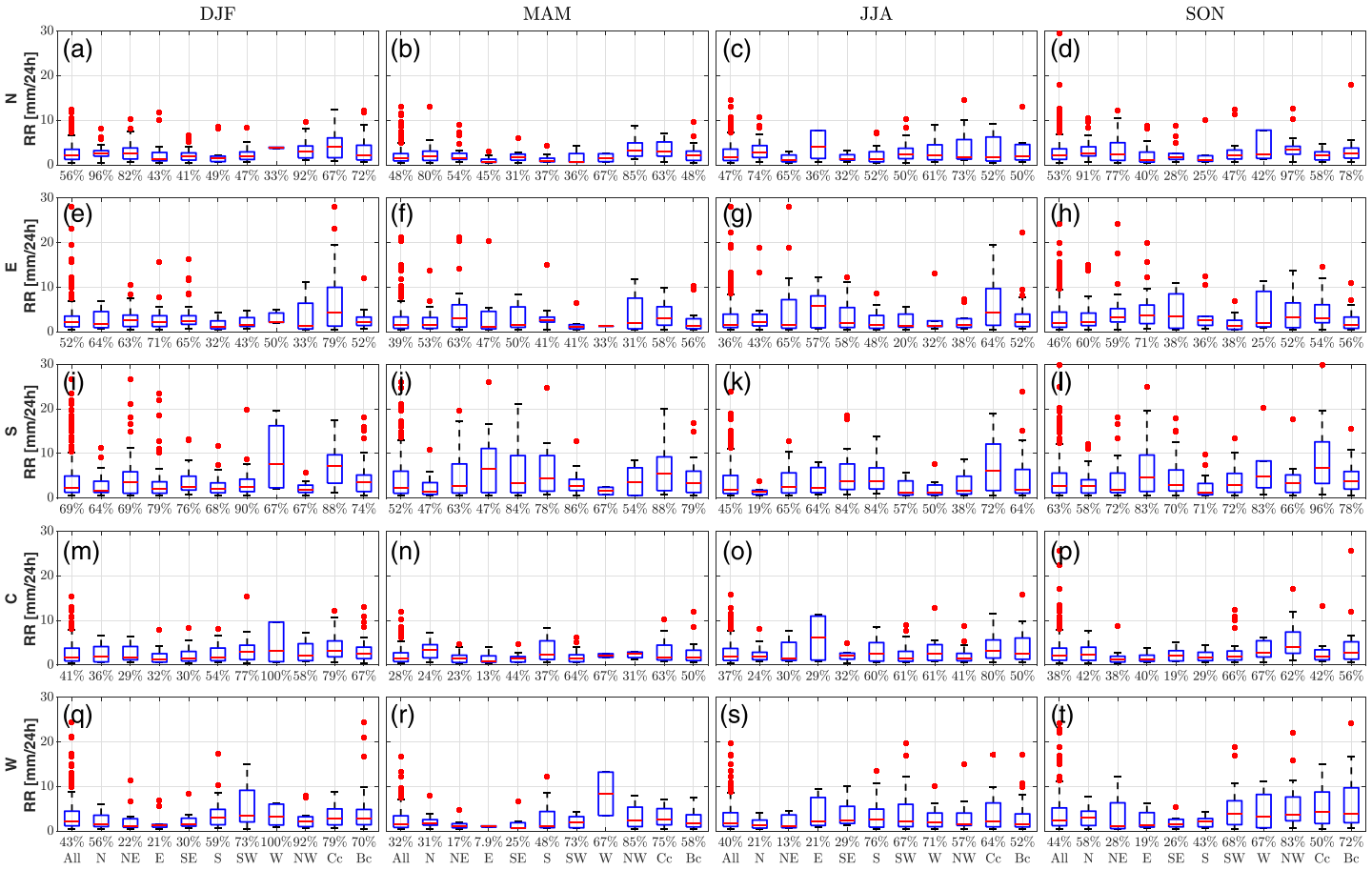

Figure 6. (a–t) Seasonal box and whisker plots of precipitation intensity, RR (mm per 24 hr), for the cyclonic atmospheric circulation (AC) types during 2013–2018 for all five stations. The solid, red line marks the median, the upper and lower edges of the blue box the 75th and 25th percentiles, the whiskers the 90th and 10th percentiles, and the red crosses are outliers. The percentages below the boxes indicate how large of a fraction of the days with a given AC type precipitate (more than 0.5 mm per 24 hr).

less cyclonic AC types compared to DJF and SON (Figure 2) and the sea ice extent being at its maximum in MAM (Figure 1).

No matter what season, there are only a handful of AC types with median precipitation intensities above 5 mm per 24 hr, reflecting the cold, dry arctic climate of Svalbard. From a societal point of view, however, the high-impact events are most often associated with the extremes and not the median. All stations have outliers with at least 25 mm per 24 h in SON. Considering both precipitation intensities (Figure 6) and 2 m air temperatures (Figure 4), we see that the AC types contributing most to precipitation in the north and east (NW, N, NE, E, SE, and Zc (Bc + Cc) in Figure 5) have subzero 10th percentile temperatures.

The high precipitation AC type at the southern, western and central stations (SW; Figure 5) has its 10th percentile DJF 2 m temperatures at zero or above (Figure 4), suggesting that these stations are more likely to experience warm winter precipitation events with rain on snow being possible.

3.3. ROS Events

3.3.1. General Statistics

This section is devoted to ROS events in DJF and their occurrence with the different AC types. Figure 7 shows the number of these events at all the five stations and the number of events with more than 3% of the land grid points below 150 m ASL (hereafter extensive events) experiencing ROS per AC type. In total, we found 57 unique ROS events at the studied stations and 49 extensive ROS events during the studied period.

Southwesterly (SW) and southerly (S) cyclonic flow have the largest contribution to ROS with 15 and 13 extensive events, respectively. These AC types also have the largest number of unique ROS events at the

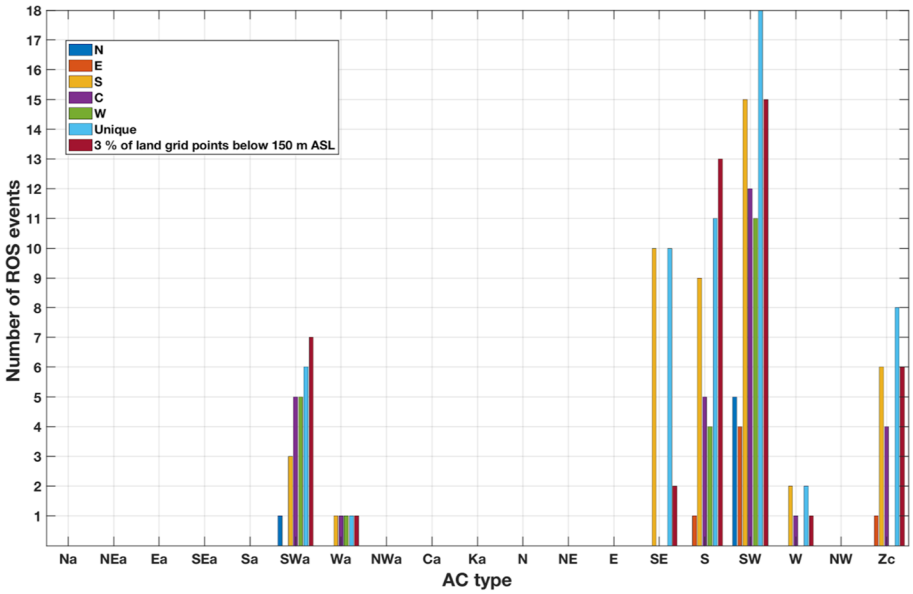

Figure 7. Bar plot showing the number of ROS events (defined in section 2.4) with the different atmospheric circulation (AC) types at the five different stations (presented in Figure 1). The light blue bar labeled unique refers to cases where a ROS event is counted only once regardless of being found at several stations. The bar labeled 3% of grid points below 150 m ASL refers to the extensive events where 3% or more of the land grid points below 150 m ASL experience a ROS event.

stations with 18 and 11 events. These numbers suggest that not all extensive ROS events are captured by the stations with the AC type S, whereas for SW the stations capture more events that have a limited spatial extent. In line with having most extensive events, SW is the only AC type with ROS events at all stations. The highest frequency, 15 events, is found at the southern station followed by 12, 11, 5, and 4 events at the central, western, northern and eastern stations, respectively. With the AC type S there are no ROS events recorded at the northern station.

After SW and S, the anticyclonic southwesterly AC type (SWa) has the highest number of extensive ROS with 7 extensive ROS events. The stations have 6 unique events, suggesting that also for SWa the stations do not capture all extensive ROS events. The AC type with a pressure center or trough over Svalbard (Zc) has 6 extensive ROS events and 8 unique events. The cyclonic southeasterly AC type (SE) has only 2 extensive ROS events despite being the second most frequent AC type to give ROS at the southern station (10 events). The westerly flow types W and Wa have 1 extensive ROS event each. Cyclonic AC types from the northerly and easterly sectors, NW, N, NE, and E, do not have any ROS events at the studied stations, nor do any anticyclonic AC types, except the above-mentioned types SWa and Wa.

Summarizing the ROS frequencies at the stations: the majority of the unique ROS events, 47 out of 57, were recorded at the southern station, whereas the northern and eastern stations display the fewest events with 6 each. At the northern station ROS events are recorded only with southwesterly flow, 5 with SW and 1 with SWa. At the eastern station 4 out of 6 ROS events occur with SW, 1 with Zc and 1 with S. The western and central stations have resembling ROS event distributions with AC type. Of these two, the central station is located at a lower latitude compared to the western station and has more ROS events. The central station has, unlike the western station, 1 ROS event with due westerly cyclonic flow (AC type W) and 4 with AC type Zc. In the south, the AC types SW, SE, and S have the highest number of ROS Events, 15, 10 and 9, respectively.

3.3.2. Spatial Distribution

We now set the point measurements at the five stations (Figure 7) into a regional perspective (Figure 8). Starting with an overview, 51% of the land grid points in AROME-Arctic experienced at least one ROS event in the winters 2013–2018. 21% of the land grid points have five or more ROS events over the same period (at least one event per season). The highest frequencies of these events are found at the southern and southwestern coasts with up to 51 ROS days over the studied period (Figure 8a). In contrast, most of the northern and

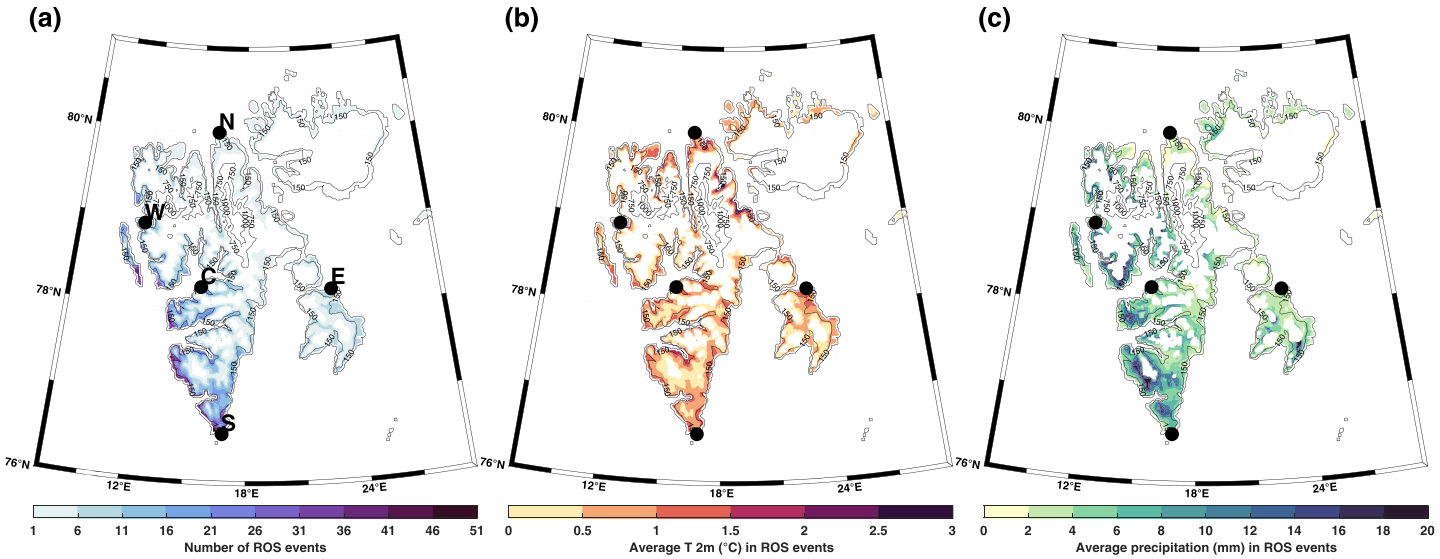

Figure 8. (a) Number of ROS events (defined in Section 2.4) over land during DJF 2013-2018, (b) average T 2 m for ROS events and (c) average daily precipitation (mm) for ROS events. The 150 m ASL terrain height contour is indicated as well in each of the panels.

northeastern regions of Svalbard experienced only 2 or less ROS events over the same period. The vast majority of the ROS events are found at altitudes below 150 m ASL, and mostly in the southern parts of the archipelago ROS events are found at higher altitudes. The daily mean temperatures for ROS events are 1–2°C below 150 m ASL and 0–1°C at higher altitudes (Figure 8b). The highest precipitation amounts during ROS events fall at the southwestern coast with a mean of around 20 mm per ROS, whereas in the east and north, the average ROS precipitation is only about 5 mm (Figure 8c).

3.3.3. Composite Analysis

Hereafter, we focus on the AC types with the largest number of extensive ROS events (Figure 7) at the five stations. The largest spatial extent of ROS events was found with the AC type SW (Figure 9b). This AC type has at least one or more ROS events at almost all coastal areas of the Svalbard archipelago during the five winters investigated. Of all AC types SW has the highest number of ROS events on the east coast of Svalbard. The anticyclonic counterpart of SW, the AC type SWa with southwesterly flow over Svalbard driven by a high-pressure ridge southeast of the archipelago (Figure S2), has ROS events concentrated more on the west coast with no cases in the northeastern parts of Svalbard (Figure 9a). As expected based on Figure 7, the AC type SE has the ROS events concentrated at the very southern tip of the archipelago (Figure 9c). With the AC type S, ROS events are found mainly at the west coast (Figure 9d). A few (below five) events are found at the southeastern coast and on the island Edgeøya, east of Spitsbergen (Figure 1). The AC type Zc has ROS events only at the southern parts of the archipelago, at both the eastern and western coasts.

In addition to the spatial ROS distributions, we have calculated composites for spatial patterns of 2 m temperature and precipitation intensities in ROS events with different AC types (Figures 9f–9j and 9k–9o). The composites are based on cases with at least 3% of the land grid points below 150 m ASL experiencing ROS, for each AC type. Starting with the temperature composites, in agreement with the definition, all the AC types have above-freezing temperatures south and west of Svalbard. All of these composites have temperatures below −10°C in the north and northeastern parts of Svalbard. When comparing to the DJF climatology (Figure 2a), we see that all four composites in Figure 9 are anomalously warm in all of the domain. The general pattern, with the coldest subzero temperatures in the northeast and above-freezing temperatures in the southwest, is very similar to the SON climatology, in all temperature composites. The coldest maritime 2 m air temperatures are found in the northwestern corner of the domain, close to the northeastern corner of Greenland.

The AC type SWa has the overall warmest temperatures, with above-freezing temperatures reaching all the way past 80°N on the west coast of Svalbard. A warm tongue of up to 4°C 2 m air temperatures reaches up to about 78°N. With the cyclone driven SW AC flow type the 2 m temperatures south of Svalbard are warmer

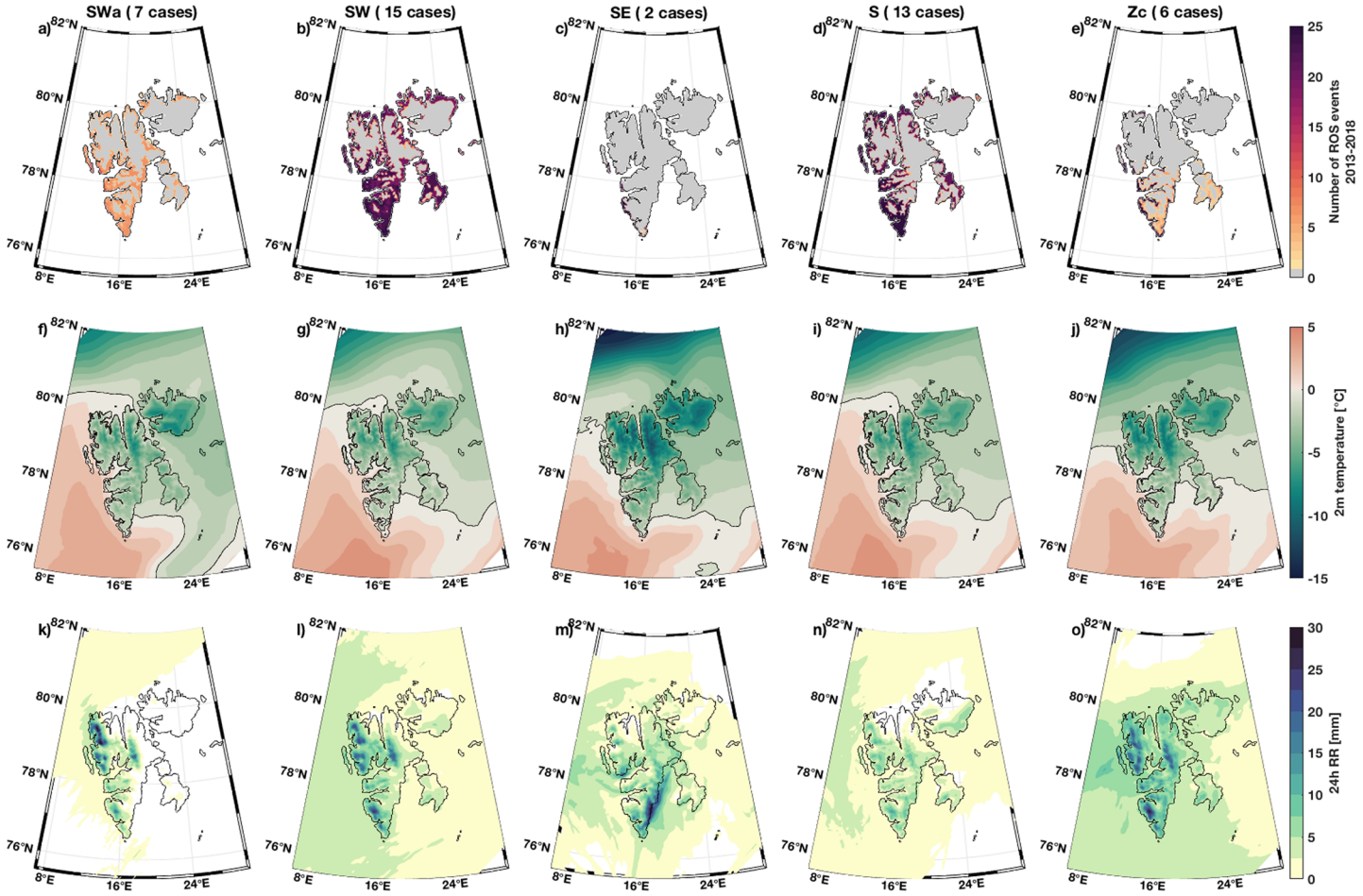

Figure 9. Number of ROS events during DJF 2013-2018 for r (a) SWa, (b) SW, (c) SE, (d) S, and (d) Cc AC types and the composites of (f–j) 2 m air temperature (°C) and (k–o) precipitation (mm per 24 hr) produced as described in the text.

compared to the SWa, but the north-south gradient is sharper and the temperatures north of 78°N are below those of the SWa composite. For the S AC type, the warm tongue on the west side of Svalbard reaches farther north than for the SW AC type, but the maximum temperatures south of Svalbard are lower. The SE AC type is the generally coldest of these composites with the mentioned warm tongue shifted to the west and off the coast of Svalbard. The temperature pattern for Zc (cyclone center or trough over Svalbard) differs from the others in the lack of the strong east-west temperature gradient, as the warmest air is distributed close to meridionally symmetrically around the southern tip of Spitsbergen.

Next, we present composites of precipitation for the AC types associated with ROS events (Figure 9, Row 3). The precipitation patterns reflect well the AC types with precipitation on the upwind side of Svalbard. An interesting detail is the difference between the AC types SWa and SW. The anticyclonic SWa has precipitation concentrated at the west coast, with the largest amounts of precipitation at the northwestern corner of Svalbard (Figure 9k). In contrast, the cyclone-driven SW AC type has precipitation over Fram Strait, west of Svalbard, that reaches both north and south of the archipelago. Like with SWa, SW has the highest precipitation rates on the windward side of the mountainous parts of Svalbard. These patterns suggest that the SWa AC type precipitation patterns is strongly controlled by the orography with coastal precipitation due to forced lifting. In contrast, the cyclonic SW pattern is more typical of an extratropical cyclone with frontal precipitation.

The geographical east-west distribution of precipitation for the AC type SE is close to opposite to that of SW, with precipitation along the east coast. The southerly flow (S AC type) gives low precipitation intensities over most of Svalbard, except the very north (Figure 9n). Further, the precipitation composite of Zc agrees well

with an extratropical cyclone being centered over the archipelago. The even precipitation distribution over Svalbard as well as south and west of the archipelago indicates the warm sector of the cyclone.

4. Discussion

The seasonal climatologies shown in Figure 3 well demonstrate the large local variability of 2 m temperature and precipitation within Svalbard. There is a strong, zonal temperature gradient across the archipelago, especially in SON (Figure 3d), driven by the warm West Spitsbergen Current running northward along the west coast (Carmack et al., 2015). This variability is not captured by studies utilizing only west coast observations. Given the high 2.5 km horizontal grid spacing of AROME-Arctic, the model provides valuable insight to the local variability in temperature and precipitation patterns beyond what can be identified on the basis of global model or reanalysis products currently available. The heterogeneity in meteorological conditions across Svalbard is clear in the differences in the temperature and precipitation medians and their variability between the 5 stations studied (Figures 4–6). The large differences in precipitation intensities, with differing AC, on the upwind side demonstrates that AROME-Arctic has a great potential to increase the knowledge of both local and regional variability of the consequences of a warmer and wetter climate in this region.

We are aware of the uncertainties in purely model based studies, especially in regions with a highly complex terrain and strong air-sea-ice interaction like Svalbard (Kilpeläinen et al., 2011; Kilpeläinen et al., 2012; Mäkiranta et al., 2011). However, based on our validation of the model's performance with respect to temperature and precipitation (section 2.5) and recent results presented by others (Bengtsson et al., 2017; Müller, Batrak, et al., 2017; Müller, Homleid, et al., 2017), we conclude that AROME-Arctic is suitable for studying spatial variability on a local scale. We also note that given the complex terrain in Svalbard, the specific location of an AWS may not always be well represented in the model topography.

Several studies have pointed out the importance of sea ice for both local, regional and larger-scale climate (Vihma, 2014). The presence of sea ice greatly reduces oceanic heat and moisture fluxes into the lowermost atmosphere. Further, along these lines we hypothesize that the seasonal variability in temperature and precipitation across the different AC types is partly driven by sea ice extent in the sense that winter sea ice cover affects the upwind conditions by strongly reducing the air-sea heat and water vapor exchange when present. The small variability in temperature and precipitation across the summertime AC types is probably a sum of the lower sea ice overage close to Svalbard and the minor difference of surface temperatures of sea ice and open ocean in summer.

In addition, we argue that sea ice exerts an even stronger control on local precipitation than on temperature. For example, much higher precipitation rates north of Svalbard with the NE AC type in DJF compared to MAM are visible only at the northern station, having on average an ice-free coast in DJF but not in MAM (Figure 5). The sharp temperature contrast between the open sea and sea ice accommodates for cold air outbreaks and shower bands in situations with off-ice flow (as well known on the basis of studies of analogous off-shore flows over the U.S. Great Lakes; (Peace & Sykes, 1966) and the Gulf of Finland (Mazon et al., 2015), explaining the individual high precipitation events at the northern station with northerly flow in DJF (Figures 5a and 6a).

We argue that ROS events are predominantly driven by advection of warm air masses from the southerly sector and are not so sensitive to the presence of sea ice. A daily mean temperature at or above 0°C requires advection of warmer air masses from lower latitudes as the winter season has no direct sunlight at these latitudes. As mentioned in section 1, cyclone activity is the main atmospheric mechanism of poleward heat transport, especially in the winter with the strongest equator-to-pole temperature gradient. Most of the ROS events occur under a southwesterly flow (AC type SW), with a low-pressure system centered west-southwest of Svalbard (Figure S1). These synoptic situations typically occur with a meridional tropospheric jet stream placing Svalbard on the warm side of the jet with the whole archipelago in a warm midlatitude air mass. Contrastingly, when Svalbard is under southeasterly flow, which is the most common DJF AC type, ROS events are constrained primarily to just to the very southern parts of Spitsbergen. This is most likely because cyclonic southeasterly flow over Svalbard requires a low-pressure system positioned southwest of Svalbard. This kind of synoptical situation occurs when the jet stream is more zonal and the storm track goes into the Barents Sea, leaving Svalbard on the southern side of the jet stream and in the arctic air mass.

To put our findings on ROS events in context, we acknowledge that we are not the first to study these events in Svalbard. A number of recent studies (Dobler et al., 2019; Hanssen-Bauer et al., 2019 and Peeters et al., 2019) have reached similar conclusions. Both Hanssen-Bauer et al. (2019) and Dobler et al. (2019) found that ROS events are a relatively widespread phenomenon in Svalbard, and most common during southwesterly synoptic flow. Studying the regions close to Ny-Ålesund (W station in this work) and Svalbard Airport (C station in this work), Peeters et al. (2019) found that ROS events occur over large spatial scales. These results support our conclusions and build confidence in our model-based results. For future studies, utilization of satellite based snow cover or albedo products could be used to identify ROS events.

5. Conclusions

An evident feature of the present warm and wet winter conditions in Svalbard is the large number and spatial extent of ROS events. These events, which according to our definition have a daily mean 2 m air temperature at or above freezing (0°C) and precipitation at least 1 mm per 24 hr, have potentially large impacts on ecosystems, the cryosphere and infrastructure. Our results demonstrate that most of the coastal areas have experienced several of these events over the studied period, but they are most frequent in the southern and southwestern parts of the archipelago.

We found that southwesterly flow makes the largest contribution to wintertime ROS events, both in number and spatial coverage. This AC type, both cyclone and anticyclone driven, is also associated with the warmest air masses along the west coast of Svalbard with 2 m air temperatures of up to 5°C south of Svalbard. These composites are 5°C to 10°C warmer than climatology. The precipitation patterns are in general strongly controlled by the orography, especially with the anticyclonic flow SWa. At the southern station the SE AC type is a remarkable contributor to the number of ROS events, but the warm and wet air masses do not make it farther north in this flow type.

To date, ROS events in Svalbard have been mostly considered from the perspective of their consequences on the ecosystems, cryosphere, and society (Hansen et al., 2014, 2019). In this work we have presented a climatology of these high-impact events in the present climate, and the AC types driving them. Our results allow these ROS events to be considered from a climatological point of view and not only based on individual cases and their consequences. A natural next step would be to study trends in both frequency and intensity of these warm and wet wintertime ROS events. Unfortunately, this is not possible with the presently available AROME-Arctic data set, as it only provides data since October 2012. In the future, high-resolution atmospheric reanalyses will be available for this purpose.

We have also studied the present 2 m temperature and precipitation climate in Svalbard and its temporal variability. The seasonal variations seem to be partly driven by both local and regional sea ice extent, with the largest variability at the stations in the north and the east. We hypothesize that the orography of Svalbard and sea ice cover are the main contributors to the large spatial variability in temperature and precipitation patterns associated with a certain AC type. Our results show that the high-resolution numerical weather prediction model AROME-Arctic is a useful tool to study spatial variability on both regional and local scales in Svalbard. Due to the sparse coverage of observational data in the northern and eastern parts of Svalbard, these alone do not provide sufficient information about the spatial variability.

Data Availability Statement

The AROME-Arctic data are available online (https://thredds.met.no/thredds/catalog/aromearcticarchive/catalog.html).

Acknowledgments
The work was supported by the Academy of Finland (Contract 317999). We want to thank two anonymous reviewers for constructive comments that helped us improve this manuscript.

References

Aagaard, K., & Greisman, P. (1975). Toward new mass and heat budgets for the Arctic Ocean. *Journal of Geophysical Research*, *80*(27), 3821–3827. https://doi.org/10.1029/JC080i027p03821

Bauer, P., & Jung, T. (2016). Editorial for the quarterly journal's special issue on polar prediction. *Quarterly Journal of the Royal Meteorological Society*, *142*(695), 537–538. https://doi.org/10.1002/qj.2639

Bengtsson, L., Andrae, U., Aspelien, T., Batrak, Y., Calvo, J., de Rooy, W., et al. (2017). The HARMONIE–AROME model configuration in the ALADIN–HIRLAM NWP system. *Monthly Weather Review*, *145*(5), 1919–1935. https://doi.org/10.1175/MWR-D-16-0417.1

Bieniek, P. A., Bhatt, U. S., Walsh, J. E., Lader, R., Griffith, B., Roach, J. K., & Thoman, R. L. (2018). Assessment of Alaska rain-on-snow events using dynamical downscaling. *Journal of Applied Meteorology and Climatology*, *57*(8), 1847–1863. https://doi.org/10.1175/JAMC-D-17-0276.1

Bromwich, D. H., Wilson, A. B., Bai, L.-S., Moore, G. W. K., & Bauer, P. (2016). A comparison of the regional Arctic system reanalysis and the global ERA-interim reanalysis for the Arctic: The Arctic system reanalysis. *Quarterly Journal of the Royal Meteorological Society*, *142*(695), 644–658. https://doi.org/10.1002/qj.2527

Carmack, E., Polyakov, I., Padman, L., Fer, I., Hunke, E., Hutchings, J., et al. (2015). Toward quantifying the increasing Role of oceanic heat in sea ice loss in the new Arctic. *Bulletin of the American Meteorological Society*, *96*(12), 2079–2105.

Dai, A., Luo, D., Song, M., & Liu, J. (2019). Arctic amplification is caused by sea-ice loss under increasing CO_2. *Nature Communications*, *10*(1), 121. https://doi.org/10.1038/s41467-018-07954-9

Dobler, A., Førland, E. J. & Isaksen, K. (2019). Present and future heavy rainfall statistics for Svalbard—Background-report for Climate in Svalbard 2100. NCCS-Report 3/2019 (www.klimaservicesenter.no).

Donlon, C. J., Martin, M., Stark J., Roberts-Jones, J., Fiedler E., Wimmer W. (2012). The Operational Sea Surface Temperature and Sea Ice Analysis (OSTIA) system. *Remote Sensing of Environment*, *116*, 140–158. https://doi.org/10.1016/j.rse.2010.10.017

Forbes, B. C., Kumpula, T., Meschtyb, N., Laptander, R., Macias-Fauria, M., Zetterberg, P., et al. (2016). Sea ice, rain-on-snow and tundra reindeer nomadism in Arctic Russia. *Biology Letters*, *12*(11), 20160466. https://doi.org/10.1098/rsbl.2016.0466

Førland, E. J., Benestad, R., Hanssen-Bauer, I., Haugen, J. E., & Skaugen, T. E. (2012). Temperature and precipitation development at Svalbard 1900–2100. *Advances in Meteorology*, *2011*, 1–14. https://doi.org/10.1155/2011/893790

Gjelten, H. M., Nordli, Ø., Isaksen, K., Førland, E. J., Sviashchennikov, P. N., Wyszynski, P., et al. (2016). Air temperature variations and gradients along the coast and fjords of western Spitsbergen. *Polar Research*, *35*(1), 29878. https://doi.org/10.3402/polar.v35.29878

Graham, R. M., Cohen, L., Petty, A. A., Boisvert, L. N., Rinke, A., Hudson, S. R., et al. (2017). Increasing frequency and duration of Arctic winter warming events. *Geophysical Research Letters*, *44*, 6974–6983. https://doi.org/10.1002/2017GL073395

Graversen, R. G., Langen, P. L., & Mauritsen, T. (2014). Polar amplification in CCSM4: Contributions from the lapse rate and surface albedo feedbacks. *Journal of Climate*, *27*(12), 4433–4450.

Hansen, B. B., Gamelon, M., Albon, S. D., Lee, A. M., Stien, A., Irvine, R. J., et al. (2019). More frequent extreme climate events stabilize reindeer population dynamics. *Nature Communications*, *10*(1), 1616. https://doi.org/10.1038/s41467-019-09332-5

Hansen, B. B., Isaksen, K., Benestad, R. E., Kohler, J., Pedersen, Å. Ø., Loe, L. E., et al. (2014). Warmer and wetter winters: Characteristics and implications of an extreme weather event in the High Arctic. *Environmental Research Letters*, *9*(11), 114021. https://doi.org/10.1088/1748-9326/9/11/114021

Hanssen-Bauer, I., Førland, E.J., Hisdal, H., Mayer, S., Sandø, A. B. and Sorteberg, A. (2019). Climate in Svalbard 2100—A knowledge base for climate adaptation. NCCS Report no. 1/2019 (www.klimaservicesenter.no)

Isaksen, K., Nordli, Ø., Førland, E. J., Łupikasza, E., Eastwood, S., & Niedźwiedź, T. (2016). Recent warming on Spitsbergen—Influence of atmospheric circulation and sea ice cover. *Journal of Geophysical Research: Atmospheres*, *121*, 11,913–11,931. https://doi.org/10.1002/2016JD025606

Kilpeläinen, T., Vihma, T., Manninen, M., Sjöblom, A., Jakobson, E., Palo, T., & Maturilli, M. (2012). Modelling the vertical structure of the atmospheric boundary layer over Arctic fjords in Svalbard. *Quarterly Journal of the Royal Meteorological Society*, *138*(668), 1867–1883. https://doi.org/10.1002/qj.1914

Kilpeläinen, T., Vihma, T., & Olafsson, H. (2011). Modelling of spatial variability and topographic effects over Arctic fjords in Svalbard. *Tellus A*. https://doi.org/10.3402/tellusa.v63i2.15775

Køltzow, M., Casati, B., Bazile, E., Haiden, T., & Valkonen, T. (2019). An NWP model Intercomparison of surface weather parameters in the European Arctic during the year of polar prediction special observing period northern hemisphere 1. *Weather and Forecasting*, *34*(4), 959–983. https://doi.org/10.1175/WAF-D-19-0003.1

Koyama, T., Stroeve, J., Cassano, J., & Crawford, A. (2017). Sea ice loss and Arctic cyclone activity from 1979 to 2014. *Journal of Climate*, *30*(12), 4735–4754. https://doi.org/10.1175/JCLI-D-16-0542.1

Lamb, H.H., 1972: British Isles weather types and a register of daily sequence of circulation patterns, 1861-1971. Geophysical Memoir 116, HMSO, London, 85pp.

Łupikasza, E. B., Ignatiuk, D., Grabiec, M., Cielecka-Nowak, K., Laska, M., Jania, J., et al. (2019). The role of winter rain in the glacial system on Svalbard. *Water*, *11*(2), 334.

Mäkiranta, E., Vihma, T., Sjöblom, A., & Tastula, E.-M. (2011). Observations and modelling of the atmospheric boundary layer over sea-ice in a Svalbard Fjord. *Boundary-Layer Meteorology*, *140*(1), 105–123. https://doi.org/10.1007/s10546-011-9609-1

Mazon, J., Niemelä, S., Pino, D., Savijärvi, H., & Vihma, T. (2015). Snow bands over the Gulf of Finland in wintertime. *Tellus A: Dynamic Meteorology and Oceanography*, *67*(1), 25102. https://doi.org/10.3402/tellusa.v67.25102

McCabe, G. J., Clark, M. P., & Hay, L. E. (2007). Rain-on-snow events in the Western United States. *Bulletin of the American Meteorological Society*, *88*(3), 319–328. https://doi.org/10.1175/bams-88-3-319

Müller, M., Batrak, Y., Kristiansen, J., Køltzow, M. A. Ø., Noer, G., & Korosov, A. (2017). Characteristics of a convective-scale weather forecasting system for the European Arctic. *Monthly Weather Review*, *145*(12), 4771–4787. https://doi.org/10.1175/MWR-D-17-0194.1

Müller, M., Homleid, M., Ivarsson, K.-I., Køltzow, M. A. Ø., Lindskog, M., Midtbø, K. H., et al. (2017). AROME-MetCoOp: A Nordic convective-scale operational weather prediction model. *Weather and Forecasting*, *32*(2), 609–627. https://doi.org/10.1175/WAF-D-16-0099.1

Niedźwiedź, T. (2013). The atmospheric circulation. In A. A. Marsz, & A. Styszyńska (Eds.), *Climate and climate change at Hornsund, Svalbard*, (pp. 57–74). Gdynia, Poland: Gdynia Maritime Univ.

Nordli, Ø., Przybylak, R., Ogilvie, A. E. J., & Isaksen, K. (2014). Long-term temperature trends and variability on Spitsbergen: The extended Svalbard airport temperature series, 1898–2012. *Polar Research*, *33*(1), 21349. https://doi.org/10.3402/polar.v33.21349

Onarheim, I. H., Smedsrud, L. H., Ingvaldsen, R. B., & Nilsen, F. (2014). Loss of sea ice during winter north of Svalbard. *Tellus A: Dynamic Meteorology and Oceanography*, *66*(1), 23933. https://doi.org/10.3402/tellusa.v66.23933

Overland, J. E., & Wang, M. (2016). Recent extreme Arctic temperatures are due to a split polar vortex. *Journal of Climate*, *29*(15), 5609–5616. https://doi.org/10.1175/JCLI-D-16-0320.1

Park, D.-S. R., Lee, S., & Feldstein, S. B. (2015). Attribution of the recent winter sea ice decline over the Atlantic sector of the Arctic Ocean. *Journal of Climate*, *28*(10), 4027–4033. https://doi.org/10.1175/JCLI-D-15-0042.1

Peace, R. L., & Sykes, R. B. (1966). MESOSCALE study of a lake effect snow storm. *Monthly Weather Review*, *94*(8), 495–507.

Peeters, B., Pedersen, Å. Ø., Loe, L. E., Isaksen, K., Veiberg, V., Stien, A., et al. (2019). Spatiotemporal patterns of rain-on-snow and basal ice in high Arctic Svalbard: Detection of a climate-cryosphere regime shift. *Environmental Research Letters*, *14*(1), 015002. https://doi.org/10.1088/1748-9326/aaefb3

Pithan, F., & Mauritsen, T. (2014). Arctic amplification dominated by temperature feedbacks in contemporary climate models. *Nature Geoscience*, *7*(3), 181–184. https://doi.org/10.1038/ngeo2071

Rinke, A., Maturilli, M., Graham, R. M., Matthes, H., Handorf, D., Cohen, L., et al. (2017). Extreme cyclone events in the Arctic: Wintertime variability and trends. *Environmental Research Letters*, *12*(9), 094006. https://doi.org/10.1088/1748-9326/aa7def

Rudeva, I., & Simmonds, I. (2015). Variability and trends of global atmospheric frontal activity and links with large-scale modes of variability. *Journal of Climate*, *28*(8), 3311–3330. https://doi.org/10.1175/JCLI-D-14-00458.1

Schlichtholz, P. (2018). Climate impacts and Arctic precursors of changing storm track activity in the Atlantic-Eurasian region. *Scientific Reports*, *8*(1), 17786. https://doi.org/10.1038/s41598-018-35900-8

Serreze, M. C., Barrett, A. P., Stroeve, J. C., Kindig, D. N., & Holland, M. M. (2008). The emergence of surface-based Arctic amplification. *The Cryosphere Discussions*, *2*(4), 601–622. https://doi.org/10.5194/tcd-2-601-2008

Serreze, M. C., & Barry, R. G. (2011). Processes and impacts of Arctic amplification: A research synthesis. *Global and Planetary Change*, *77*(1-2), 85–96. https://doi.org/10.1016/j.gloplacha.2011.03.004

Serreze, M. C., Crawford, A. D., & Barrett, A. P. (2015). Extreme daily precipitation events at Spitsbergen, an Arctic Island: EXTREME PRECIPITATION EVENTS AT SPITSBERGEN. *International Journal of Climatology*, *35*(15), 4574–4588. https://doi.org/10.1002/joc.4308

Smedsrud, L. H., Esau, I., Ingvaldsen, R. B., Eldevik, T., Haugan, P. M., Li, C., et al. (2013). The ROLE of the Barents Sea in the arctic climate system. *Reviews of Geophysics*, *51*, 415–449. https://doi.org/10.1002/rog.20017

Smedsrud, L. H., Ingvaldsen R., Nilsen J. E. Ø., Skagseth Ø. (2009). Barents Sea heat – transport, storage and surface fluxes. *Ocean Science Discussions*, *6*(2), 1437–1475. https://doi.org/10.5194/osd-6-1437-2009

Tamarin-Brodsky, T., & Kaspi, Y. (2017). Enhanced poleward propagation of storms under climate change. *Nature Geoscience*, *10*(12), 908–913. https://doi.org/10.1038/s41561-017-0001-8

Trenberth, K. E., & Stepaniak, D. P. (2003). Seamless poleward atmospheric energy transports and implications for the Hadley circulation. *Journal of Climate*, *16*(22), 3706–3722.

Vihma, T. (2014). Effects of Arctic Sea Ice Decline on Weather and Climate: A Review. *Surveys in Geophysics*, *35*(5), 1175–1214. https://doi.org/10.1007/s10712-014-9284-0

Vihma, T., Pirazzini, R., Fer, I., Renfrew, I. A., Sedlar, J., Tjernstrom, M., et al. (2014). Advances in understanding and parameterization of small-scale physical processes in the marine Arctic climate system: A review. *Atmospheric Chemistry and Physics*, *14*(17), 9403–9450. https://doi.org/10.5194/acp-14-9403-2014

Vikhamar-Schuler, D., Isaksen, K., Haugen, J. E., Tømmervik, H., Luks, B., Schuler, T. V., & Bjerke, J. W. (2016). Changes in winter warming events in the Nordic Arctic region. *Journal of Climate*, *29*(17), 6223–6244. https://doi.org/10.1175/JCLI-D-15-0763.1

Wickström, S., Jonassen, M. O., Vihma, T., & Uotila, P. (2019). Trends in cyclones in the high-latitude North Atlantic during 1979–2016. *Quarterly Journal of the Royal Meteorological Society*, *146*(727), 762–779. https://doi.org/10.1002/qj.3707

Zahn, M., Akperov, M., Rinke, A., Feser, F., & Mokhov, I. I. (2018). Trends of cyclone characteristics in the Arctic and their patterns from different reanalysis data. *Journal of Geophysical Research: Atmospheres*, *123*, 2737–2751. https://doi.org/10.1002/2017JD027439

Zhang, X., Walsh, J. E., Zhang, J., Bhatt, U. S., & Ikeda, M. (2004). Climatology and interannual variability of Arctic cyclone activity: 1948–2002. *Journal of Climate*, *17*(12), 2300–2317.

Zilitinkevich, S. S., & Esau, I. N. (2005). Resistance and heat-transfer laws for stable and neutral planetary boundary layers: Old theory advanced and re-evaluated. *Quarterly Journal of the Royal Meteorological Society*, *131*(609), 1863–1892. https://doi.org/10.1256/qj.04.143